Equilibration in Reversible Bimolecular Reactions

Arieh L. Edelstein and Noam Agmon*

Department of Physical Chemistry and the Fritz Haber Research Center, The Hebrew University, Jerusalem 91904, Israel

Fast reversible pseudo-unimolecular reactions do not approach equilibrium in the simple exponential fashion predicted by chemical rate equations. Many-body effects in bimolecular reactions have been revealed in an extensive series of Brownian simulations, showing up to three distinct phases in the approach to equilibrium. Recent theoretical developments are compared with the simulation as well as with experimental data concerning the pH effect in excited-state proton transfer to solvent.

I. Introduction and Overview

How do the concentrations of chemical species undergoing a reversible chemical reaction in solution reach equilibrium? The traditional theory of diffusion-influenced reactions[1] does not address this question, as it focuses on irreversible reactions. Chemical rate equations[2] predict that elementary pseudo-unimolecular reactions approach equilibrium exponentially. This may agree with experimental data of slow, "rate-limited" reactions. For fast reactions this is not the case.

A. Experimental Evidence for the Failure of Rate Equations. Figure 1 shows time-correlated single-photon counting (TCSPC) data[3] of reversible equilibration in excited 8-hydroxypyrene-1,3,6-trisulfonate (HPTS) at different pH values. This dye molecule transfers the hydroxy proton to water in about 125 ps following excitation to its first singlet state.[4-6] The excited HPTS base can rebind the proton very rapidly without being quenched to its ground electronic state. For the duration of the excited-state lifetime (ca. 6 ns) one observes a reversible reaction initiated by an ultrafast laser pulse. By lowering the pH one scans a range of conditions from geminate recombination (pH = 6) to a pseudo-unimolecular reaction (pH < 3).

The figure demonstrates the failure of traditional chemical kinetics quite dramatically: conventional rate equations (REs) with time-independent rate coefficients (full curves) cannot explain the experimental data. The most severe discrepancy is in the geminate limit, 0 mM of homogeneous protons. Only the initial decay is exponential, $\exp(-\kappa_d t)$, with a fixed dissociation rate coefficient, κ_d. This is followed by power-law decay over an extended time range, a behavior that cannot be accounted for by REs even if a two-step mechanism is invoked.[5]

The failure of REs for geminate reversible binding is perhaps not surprising, since this approach fails even for irreversible geminate recombination.[1] What is more surprising is that the disagreement carries over to homogeneous pseudo-first-order reactions, even at the relatively high proton concentrations shown in Figure 1. Agreement improves for the "modified" rate equations (dotted curves) involving time-dependent rate coefficients,[7] but only in the high concentration limit. This phenomenological approach does not help us understand the effects which render the simple RE approach inadequate.

B. What Is Missing in the Rate Equation Description? Classical RE involve a finite number of chemical species and kinetic steps. For the simplest kind of A + B ⇌ AB reaction one might consider only two distinct species, AB and A + B.

In reality, the dissociated A and B partners may be at a range of interparticle distances. In addition, classical REs do not take the individual microscopic identity of reacting particles into account. It is replaced by macroscopic "concentrations".

As a result, two important effects are absent in the rate equation description: (i) nonequilibrium spatial distribution of reactants[8] and (ii) competition over binding.[9] The distribution of A and B particles in space is due to the initially prevailing distribution (which is random in the present case) and to its transient variation induced by the reactive process. Competition is a many-body effect arising from the microscopic individuality of the reacting molecules. B may bind to A if A is free but will not bind to it when it is in the bound, AB, state. This differs from the mean-field assumption inherent in the RE, in which the binding rate is proportional to the average survival probability of unbound A.

C. The Simplest Bimolecular Model. In order to disentangle the different effects in a complicated many-body situation, it is prudent to choose the simplest model of a bimolecular reaction. The chosen model has a rigorous solution in the irreversible case, which may serve as a reference in analyzing reversible reactions. Our model system consists of a single, static A molecule in an infinite space in d dimensions, surrounded by randomly distributed, noninteracting B-particles of an average concentration c and a diffusion constant D. Whenever A and B reach a "contact" distance, a, they react with an intrinsic recombination rate parameter, κ_r, unless A is already bound. This is equivalent to setting $\kappa_r = 0$ for an AB + B encounter. An AB pair dissociates with an intrinsic dissociation rate parameter, κ_d, to the same "contact" separation, a.

The assumption of a single A eliminates A—A correlations by restricting attention to the pseudo-unimolecular case. B—B correlations are eliminated by the two main simplifications in this model: static A and noninteracting B's. The only B—B interaction occurs at the entrance to the "binding site", A. Since this site is assumed to be spherical, the whole problem becomes spherically symmetric. The kinetics are affected by the distribution of B's around the site and from their competition over binding.

The simplified model is nevertheless quite realistic. In the experimental system, protons are indeed in excess at low pH when many-body effects may be operative. They also diffuse nearly 1 order of magnitude faster than the organic dye molecule. In the irreversible case, it has been shown that correlations introduced by a moving A are small even in one dimension.[10,11] They are expected to be even smaller for three-
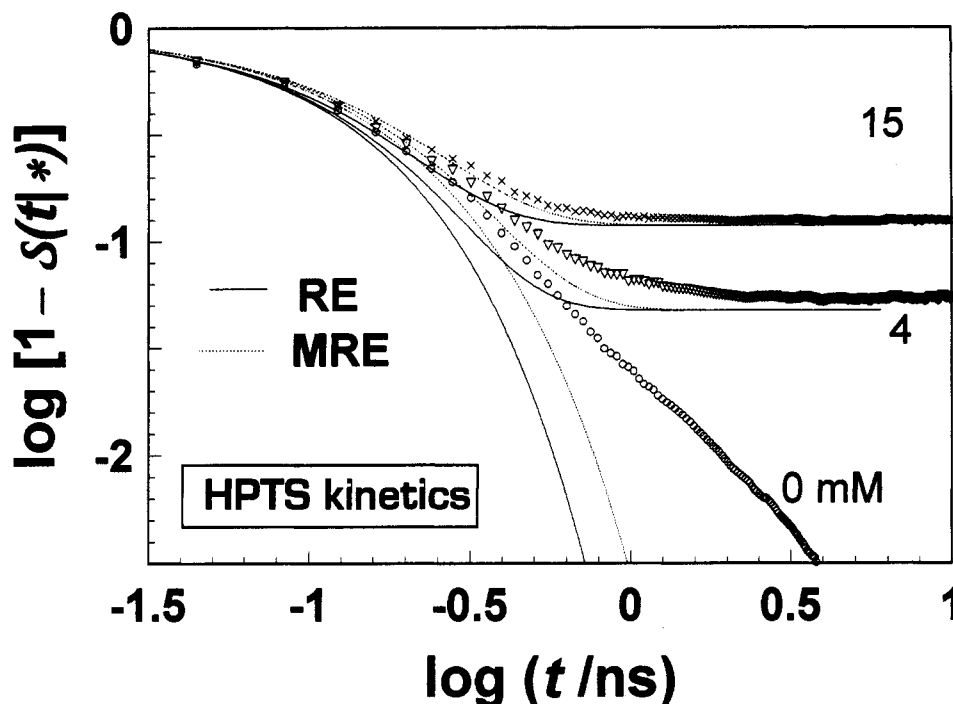

Figure 1. pH effect on excited-state proton transfer to solvent (water) from a HPTS dye molecule. Symbols are TCSPC data obtained at the three indicated concentrations of perchloric acid.[3] Experiment is compared with solutions of rate equations (eq 17) and modified rate equations (eq 19). The parameters used are listed in Table 1.

dimensional systems. Finally, protons do interact via long-range electrostatic forces. Fortunately, for the rather small concentrations (in the 10 mM range) required for demonstrating many-body effects, this B−B interaction may be replaced by an A−B potential of mean force, for example, the well-known Debye−Hückel (DH) screened Coulomb potential.

D. Two Phases of Irreversible Recombination. The survival probability in a pseudo-unimolecular reaction A + B → AB involving a static A molecule and many diffusing B's is given by the Smoluchowski theory.[12,13] An exact theory exists for the simple model in the irreversible case because in a reaction which is over upon the first A−B encounter, many-particle competition over binding cannot occur. The survival probability subsequently factors into single-particle solutions. Of the two above-mentioned effects, only the spatial B-particle distribution is reflected in the binding kinetics.

The pair dynamics dictating the reaction course may be characterized by a time-dependent rate coefficient, $k(t)$.[14] For fast reactions in three dimensions, $k(t)$ shows two characteristic phases. Starting from a high value, arising from recombination with nearby partners, it decreases as $t^{-1/2}$. This short-time behavior is governed by the initial distribution of B-particles. The initial random distribution approaches steady-state conditions in which short A−B distances are less probable. In this limit, $k(t)$ tends to a constant asymptotic value and the survival probability becomes exponential.

Many-body effects leading to asymptotic power-law decays have also been discussed for truly bimolecular (not pseudo-unimolecular) arrangements of particles.[15] The A + B → 0 (annihilation, recombination) reaction has been analyzed by starting from equal initial concentrations of randomly distributed A's and B's.[16] Two power-law regimes have been identified: At intermediate times, the average density of A (or of B) decays as $t^{-d/2}$ for $d \leq 2$ and as t^{-1} for $d \geq 3$. At long times, there is a switchover to a $t^{-d/4}$ decay if $d \leq 4$. The asymptotic behavior in this case is due to segregation into domains which are locally richer in A or in B. It depends on the exact form of the initial

distribution and, so far, has not been seen experimentally. We do not treat the reversible extension of the equal concentration problem.

E. Theoretical Approaches to Reversible Reactions. Unlike the irreversible case, in reversible pseudo-unimolecular reactions, A + B ⇌ AB, many-body competition effects do become important. In each dissociation−diffusion−recombination cycle, the original ("geminate") partner competes with the other ("homogeneous") B's for rebinding. The solution of the hierarchy of N-body diffusion equations does no longer factor into single-particle solutions.[17]

Theories requiring the solution of an effective single-particle diffusion equation can be only approximate in the reversible case. Quite a number of such approximations have been recently proposed.[7,18−40] These include the "modified rate equation" (MRE),[7,36,37] a Kirkwood-like "superposition approximation" (SA),[18,36] a "convolution approximation" (CA)[35] more adequate[7] than phenomenological "convolution kinetics",[21] a "bimolecular boundary condition"[9] approach ("chemical approximation"[36]), an "average correlation" model,[34] and a "density expansion" approach.[17] The first three approximations tend to the correct equilibrium limit and are hence suitable in analyzing both short- and long-time behaviors.[7]

The exact time dependence for equilibration can be obtained either by solving the N-particle equations (which is practical only for small N) or by simulation. Discrete-time discrete-space random walks have been used routinely to investigate irreversible diffusion-influenced reactions.[10] These methods were extended to the simple model of reversible bimolecular reactions in both one[9,36] and three dimensions.[34,37] To monitor the approach to equilibrium up to the asymptotic regime and for different concentrations and binding parameters, long stochastic trajectories over many orders of magnitude in time are required. This presents a difficulty for random-walk methods utilizing fixed time steps.

Depending on the value of the equilibrium constant, K_{eq}, the binding probability may be very close to either one or zero. Obtaining the deviation from equilibrium then requires several digit accuracy in the simulation, obtainable by averaging over

Equilibration in Reversible Bimolecular Reactions

J. Phys. Chem., Vol. 99, No. 15, 1995 **5391**

millions of stochastic trajectories. Long and accurate simulations are made possible by Brownian dynamics.[41,43] A stochastic move is determined by picking a random number from the exact single-particle probability density, available in closed form for one dimension.[38] The time step may be arbitrarily large, and just a few are required for the survival probability to approach physically acceptable values.

F. Three Phases of Reversible Dissociation. From previous partial results[40] and the comprehensive results presented below, the following picture emerges. Unlike irreversible recombination, reversible dissociation shows up to three phases in the time dependence of equilibration. At low concentrations, c, or fast dissociation (large κ_d), the binding site is mostly vacant and the competition effect is negligible. In these limits we observe only two phases which, like in the irreversible case, are due to the evolution of the B-particle distribution in space.

The short-time behavior reflects the initial condition. As in the experiment, we consider an AB molecule surrounded by a concentration c of B's, namely, one particle is initially bound and the remaining B's are randomly distributed. The initial process is therefore dissociation of AB, so that for $t \to 0$ the binding probability decays exponentially, $\exp(-\kappa_d t)$, provided that dissociation is faster than diffusion. While for irreversible recombination the long time behavior reduces to ordinary exponential kinetics, for reversible dissociation, only the short time behavior is describable by a RE.

In the limit of vanishing competition, the long-time behavior may be explained as follows: the probability of finding a vacant site, A, is given at equilibrium by $1/(1 + cK_{eq})$. Here K_{eq} is the equilibrium (recombination) constant, for which an exact expression is given below. Suppose that all particles are initially equilibrated except for one which dissociates at $t = 0$. This particle may undergo several cycles of recombination and dissociation, but eventually, it will escape to large distances. After long times the delay introduced by repetitive recombination is negligible, and so are any interactions with the site which are assumed to vanish at infinitely large separations. Hence for large t the particle's probability density approaches a Gaussian distribution. Its probability of return to the binding site at the origin is thus $(4\pi Dt)^{-d/2}$. For weak competition, one expects the long time decay of the binding probability to approach $[K_{eq}/(1 + cK_{eq})](4\pi Dt)^{-d/2}$. This result has been derived from the linearized SA.[7] It is valid at low concentrations and generalizes an earlier result obtained in the zero concentration (geminate) limit.[5]

For higher concentrations or slower dissociation, competition over binding plays an increasingly important role. The asymptotic power law still holds, but the prefactor in the square brackets is wrong. Under these conditions, a third phase of enhanced approach to equilibrium emerges at intermediate times. This enhanced decay is a many-body effect. It is during this phase that one expects to see a discrepancy between the mean-field approximations and the exact simulation results.

G. Goals. We establish the time dependence of equilibration using 1d Brownian simulations, investigate the validity of the various mean-field approximations, and determine whether many-body effects are observed under experimental conditions. Sections II and III summarize theoretical results and equations used in the sequel. This includes the structure of the N-particle equations and the mean-field approximations. Section IV presents Brownian simulation results. These involve neutral, noninteracting particles in one dimension. The simulations are compared with the three mean-field approximations: MRE, SA, and CA. One dimension is typically the most demanding, so one expects the agreement to improve in three dimensions. While three-dimensional simulations with a potential of mean

force are unavailable, the approximate solutions can be calculated under such conditions. Section V compares experiment with MRE, SA, and CA results in three dimensions with a screened DH potential.

II. Theoretical Background

We summarize the theoretical results needed for carrying out the comparison between simulation and experiment. These correspond to noninteracting point particles in 1d (simulation) and univalent ions in 3d (experiment). While all pertinent equations are given and their physical significance discussed, mathematical derivations are omitted and the reader is directed to the literature. The present section discusses rigorous results for many-body irreversible and reversible reactions, while the next section focuses on several approximations for competitive reversible binding.

A. Irreversible Reactions. Consider first a pseudo-unimolecular irreversible reaction, $A + B \to AB$, involving a single A molecule and many B-particles. If A is static and the diffusion space infinite (the "thermodynamic limit"), the Smoluchowski theory is exact and the survival probability of an unreacted A molecule is given by[12,13]

$$\mathcal{S}_{irr}(t|eq) = \exp[-c\int_0^t k(t')\, dt'] \qquad (1)$$

In our notation, $\mathcal{S}_{irr}(t|eq)$ denotes the many-body survival probability for an irreversible reaction with initially equilibrated B-particles of concentration c. Equation 1 follows from an independent-pair assumption. This assumption may be applied to other initial conditions. For example, if one particle is initially at contact, $r = a$, and the remaining particles are equilibrated, one obtains[44]

$$\mathcal{S}_{irr}(t|a) = \mathcal{S}_{irr}(t|a)\,\mathcal{S}_{irr}(t|eq) = [k(t)/\kappa_a]\mathcal{S}_{irr}(t|eq) \qquad (2)$$

Here $S_{irr}(t|a)$ denotes the single-particle solution for an initial contact pair,[35] whereas $\mathcal{S}_{irr}(t|a)$ is the analogous many-body result.

The association parameter, κ_a, determines the magnitude of the A−B recombination flux when the two particles are at their minimal separation, a (the "contact distance"). It depends on the recombination parameter, κ_r, and dimensionality, d, as follows

$$\kappa_a = \begin{cases} \kappa_r & d = 1 \\ 4\pi a^2\kappa_r & d = 3 \end{cases} \qquad (3)$$

For $d = 1$ one may set $a = 0$, but otherwise $a > 0$. In the presence of a spherically symmetric A−B interaction potential, $U(r)$, it is convenient to define

$$\kappa_V \equiv \kappa_a e^{-V(a)} \qquad (4)$$

where $V(r) \equiv U(r)/k_B T$ is the potential in units of thermal energy. The potential term in eq 4 gives rise to an "activity coefficient" on rates and equilibria of chemical reactions.

Equation 1 implies that the survival probability obeys a rate equation, $d\mathcal{S}_{irr}(t|eq)/dt = -ck(t)\mathcal{S}_{irr}(t|eq)$, albeit with a *time-dependent* rate coefficient, $k(t)$, which measures the recombination flux of A−B pairs at their contact distance. $k(t)$ is obtained from the solution of the single-particle diffusion (Smoluchowski) equation

$$\frac{\partial P(x;t)}{\partial t} = x^{1-d}\frac{\partial}{\partial x}Dx^{d-1}e^{-V(x)}\frac{\partial}{\partial x}e^{V(x)}P(x;t) \qquad (5)$$

for an initial equilibrium state

$$P(x;0|eq) = e^{-V(x)} \qquad (6)$$

and subject to the "radiation" (irreversible) boundary condition

$$k(t) \equiv \gamma_d D a^{d-1} e^{-V(a)} \frac{\partial}{\partial x} e^{V(x)} P(x;t|eq)|_{x=a} = \kappa_a P(a;t|eq) \quad (7)$$

γ_d is a geometric factor, which equals 4π for $d = 3$ and 1 for $d = 1$ *provided* that (like in our simulations) particles may enter the trap from one side only (i.e., $x \geq 0$). Note that $P(x;t)$ is not normalized and hence dimensionless. To remind us of this fact, an uppercase P is used. $k(t)$ decreases with time as closely separated A−B pairs are depleted by reaction.

The expression for $k(t)$ depends on the dimensionality, d.[14] In 1d and in the absence of an interaction potential

$$k(t) = \kappa_r \exp(\kappa_r^2 t/D) \, \mathrm{erfc}(\kappa_r \sqrt{t/D}) \sim \sqrt{D/\pi^2 t} \quad (8a)$$

Here D is the relative A−B diffusion coefficient and erfc is the complementary error function. The above expression is valid for B's located on one side of the origin. The approximate expression arises from the large z limit of the error function, $\exp(z^2) \, \mathrm{erfc}(z) \sim 1/\pi z$. As $t \rightarrow \infty$, $k(t)$ vanishes so that a steady-state solution does not exist in one dimension.

In 3d with a spherically symmetric interaction potential, $U(r)$, one has for large t

$$k(t) = 4\pi D a_{eff}[1 + \gamma a_{eff} \exp(\gamma^2 Dt) \, \mathrm{erfc}(\gamma \sqrt{Dt})]$$

$$\sim 4\pi D a_{eff}[1 + a_{eff}/\sqrt{\pi^2 Dt}] \qquad (8b)$$

The "effective contact distance", a_{eff}, is related to the actual contact, distance, a, by

$$a_{eff} \equiv a_e \kappa_V / (4\pi D a_e + \kappa_V) \qquad (9a)$$

$$a_e^{-1} \equiv \int_a^\infty \exp[V(r)] r^{-2} \, dr \qquad (9b)$$

$$\gamma \equiv 1/(a_e - a_{eff}) \qquad (9c)$$

For finite times, eq 8b is exact only when $V(r) = 0$, i.e., $a_e = a$. For fast, diffusion-limited reactions $a_{eff} \rightarrow a_e$ and γa_{eff} is very large. For slow reactions $a_{eff} \rightarrow \kappa_V/4\pi D \ll 1$ so that $k(t) \rightarrow \kappa_V$. In this limit $S_{irr}(t|eq) = \exp(-c\kappa_V t)$, the conventional kinetic result.

The expression for $k(t)$ is again simplified using the asymptotic expansion for the error function. It shows two phases: a transient phase where $k(t)$ decreases approximately as $t^{-1/2}$ and a constant steady-state limit, $4\pi D a_{eff}$, when the survival probability, eq 1, decays exponentially. These phases are due to the initial, random distribution and the final steady-state distribution of B's around the site. As long as A is static and the particles are noninteracting, the survival probability is expressible in terms of the single-particle solution, $k(t)$. Thus for the simple model in the irreversible limit the many-body dynamics are uncoupled.

B. Reversible Reactions. When the reaction is reversible the B-particles are no longer independent even if the trap, A, is static. This is because the binding of one B affects the binding probability of other B's. Unlike the irreversible case, the exact description of N particles involves coupled diffusion equations in N-coupled degrees of freedom (the A−B distances). While the exact many-body equations are given elsewhere,[17] we briefly review the physics behind these equations.
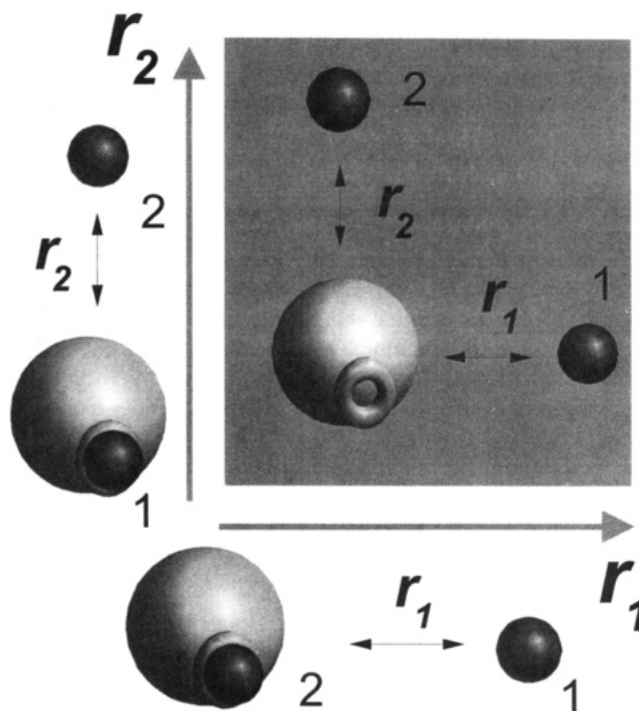

Figure 2. Schematic representation of two-particle binding to an active site.

To understand the structure of the many-body equations, consider the cases of $N = 1$ and 2. The single-particle equations are those of a reversible geminate pair.[4] The (normalized) probability density, $p(x;t)$, for an A−B pair to be separated a distance x by time t obeys the Smoluchowski equation 5 for $a \leq x \leq x_m$. The irreversible boundary condition, eq 7, is modified to a "back-reaction" (reversible) boundary condition

$$\gamma_d D a^{d-1} e^{-V(a)} \frac{\partial}{\partial x} e^{V(x)} p(x;t)|_{x=a} = \kappa_a p(a;t) - \kappa_d[1 - S(t)]$$
$$(10)$$

The survival probability for an unreacted pair is defined by

$$S(t) \equiv \gamma_d \int_a^{x_m} p(x;t) x^{d-1} \, dx \qquad (11)$$

so that the binding probability is $1 - S(t)$.

The situation for $N = 2$ is demonstrated in Figure 2. In this figure, A is depicted as a big sphere with a single binding site while the particles, B, are the two small spheres. Three different situations are possible, leading to three coupled diffusion equations: (i) both particles are free; (ii) particle B_1 is bound while B_2 is free; or (iii) particle B_2 is bound and B_1 is free. In the first case there are two distances r_i separating A and a given B. This situation is described by diffusion of a single point in the (r_1, r_2) plane with back-reaction (reversible) boundary conditions when either $r_i = a$. The other two cases involve one bound particle with the other free and diffusing. The number of degrees of freedom is reduced to one namely, the distance of the free particle from the trap. It is described by diffusion on a line with dissociation and recombination terms that couple it to the 2d equation, case (i). Simultaneous binding of both particles is, of course, excluded since we are dealing with a "single-particle trap".

Generalizing to N particles,[17] competitive reversible binding involves one N-dimensional diffusion equation coupled to N equations of dimension $N - 1$. The high dimensionality of the problem means it cannot be solved exactly even numerically. One recourses either to approximations of reduced dimensionality or to stochastic simulations. These will be described below.

Equilibration in Reversible Bimolecular Reactions

J. Phys. Chem., Vol. 99, No. 15, 1995 **5393**

C. Equilibrium and "Generalized Mass Action". While the exact many-body equations cannot be solved, their equilibrium limit is the same as that of the chemical rate equations[17]

$$\mathcal{S}_{eq} = \mathcal{S}(\infty) = 1/(1 + cK_{eq}) \qquad (12a)$$

$$K_{eq} \equiv \kappa_V/\kappa_d \qquad (12b)$$

Here K_{eq} is the (recombination) equilibrium coefficient and κ_V is defined in eq 4.

Equation 12 shows that K_{eq} obeys the "mass action" law

$$K_{eq} = (1 - \mathcal{S}_{eq})/(c\mathcal{S}_{eq}) \qquad (13)$$

This classical result can be generalized to the time domain,[35] where it relates the many-body survival probabilities for two different initial conditions: (i) a vacant site surrounded by equilibrated particles, or (ii) one particle bound and the other particles equilibrated. The survival probabilities for these two cases, denoted by $S(t|eq)$ and $S(t|*)$, respectively, are related by the "generalized mass action" (GMA) law

$$K_{eq} = [1 - \mathcal{S}(t|eq)]/[c\mathcal{S}(t|*)] \qquad (14)$$

which can be proven from detailed balancing.[17] As $t \to \infty$ the GMA reduces to the ordinary mass action law, eq 13. Using the GMA and eq 12a, the deviation from equilibrium for the two initial conditions is related by

$$\mathcal{S}_{eq} - \mathcal{S}(t|*) = [\mathcal{S}(t|eq) - \mathcal{S}_{eq}]/cK_{eq} \qquad (15)$$

In the experiment one starts from the bound state, $\mathcal{S}(0|*) = 0$, whereas in the simulations we typically begin from the unbound state, $\mathcal{S}(0|eq) = 1$. Moreover, some of the approximations, such as the SA, can only be formulated for the unbound state. It is therefore convenient to have an exact expression relating these two initial conditions.

III. Approximations

In this section we summarize three approximations used below to compare with simulation and experiment. These approximations (a) tend to the correct equilibrium limit (eq 12a), (b) obey GMA (eq 14), and (c) reduce to the correct irreversible solution when $\kappa_d = 0$ (eq 1). Two of the approximations (CA and SA) also reduce to the correct (reversible) geminate pair solution in the limit of infinite dilution, $c = 0$. It is therefore not surprising that the latter turn out to be the most useful in analyzing experiment.

Since the three approximations are conveniently discussed in the work of Szabo,[7] we only give the final results below. For pseudo-unimolecular reactions, $\mathcal{S}(t) = [A]/[A]_0$ is the survival probability of a vacant trap (unreacted A molecule) and $c = [B]$ is the (constant) concentration of B-particles. The binding probability is hence $1 - \mathcal{S}(t) = [AB]/[A]_0$. Whenever the initial condition is not specified, the result is assumed valid for any initial condition.

A. Rate and Modified Rate Equations. Conventional rate equation (RE) description of a reversible reaction involves two time-independent rate parameters, κ_a and κ_d, and no spatial dependencies of particle densities

$$d[A]/dt = -\kappa_V[A][B] + \kappa_d[AB] \qquad (16a)$$

$$d\mathcal{S}(t)/dt = -c\kappa_V\mathcal{S}(t) + \kappa_d[1 - \mathcal{S}(t)] \qquad (16b)$$

The second equation is just the pseudo-unimolecular limit of the first. Its solution depicts an exponential decay to equilibrium

$$\mathcal{S}(t|*) = \mathcal{S}_{eq}\{1 - \exp[-(c\kappa_V + \kappa_d)t]\} \qquad (17)$$

with $\mathcal{S}_{eq}$ and κ_V given in eqs 12a and 4, respectively. This solution evidently tends to the correct equilibrium limit. From the corresponding solution for $\mathcal{S}(0) = 1$ one verifies that the GMA is obeyed at all times. However, the RE does not approach the correct limit when either $\kappa_d \to 0$ or $c \to 0$. The full curves in Figure 1 indeed show that eq 17 is quite inadequate.

A "modified rate equation" (MRE) has been suggested by Szabo:[7,37]

$$dS(t)/dt = [k(t)/\kappa_V]\{-c\kappa_V\mathcal{S}(t) + \kappa_d[1 - \mathcal{S}(t)]\} \quad (18)$$

where $k(t)$ is the irreversible time-dependent rate coefficient given by eq 8. This may be solved analytically:[7]

$$\mathcal{S}(t|*) = \mathcal{S}_{eq}\{1 - \exp[-(c + K_{eq}^{-1})\int_0^t k(t')dt']\} \quad (19)$$

A similar result may be obtained for an initially unbound state. The MRE also obeys the GMA law and tends to the correct $t \to \infty$ limit. Unlike the RE, it does become exact in the irreversible limit, namely, $\mathcal{S}(t|eq) \to \mathcal{S}_{irr}(t|eq)$ as $\kappa_d \to 0$, see eq 1. However, the MRE is incorrect in the geminate-pair limit, $c \to 0$.

B. Convolution Approximation. The "convolution approximation" (CA) involves solving numerically the convolution relation[35]

$$\mathcal{S}(t|*) = \kappa_d\int_0^t [1 - \mathcal{S}(t'|*)]\mathcal{S}_{irr}(t - t'|a)\,dt' \qquad (20a)$$

$$\mathcal{S}(t|eq) = \mathcal{S}_{irr}(t|eq) + \kappa_d\int_0^t [1 - \mathcal{S}(t'|eq)]\mathcal{S}_{irr}(t - t'|a)\,dt' \qquad (20b)$$

$\mathcal{S}_{irr}(t|eq)$ and $\mathcal{S}_{irr}(t|a)$ are the survival probabilities for irreversible recombination, eqs 1 and 2 with $k(t)$ from eq 8. The physical justification to eq 20 is as follows: At time t, a particle is bound with probability $[1 - \mathcal{S}(t)]$. The fraction dissociated between t and $t + dt$ is thus $\kappa_d[1 - \mathcal{S}(t)]\,dt$. Once dissociated, the bound state is reached if one of the free particles binds without subsequent dissociation. The latter process is an irreversible recombination from contact.

The approximation is in the assumption that by the time a particle dissociates all other particles have attained their equilibrium distribution, a situation described by the function $\mathcal{S}_{irr}(t|a)$. This is best justified for slow dissociation. Indeed, when $\kappa_d = 0$, eq 20b reduces to $\mathcal{S}(t|eq) = \mathcal{S}_{irr}(t|eq)$. By taking Laplace transforms,[35] one may show that eqs 20 tend to the same equilibrium limit of eq 12a and that the GMA is obeyed. Finally, the convolution relations are rigorous in the geminate-pair limit.[35] Therefore, the CA reduces to the correct limiting behaviors in all three cases: $t \to \infty$, $\kappa_d \to 0$, *and* $c \to 0$.

C. Superposition Approximation. In the SA, the many-body survival probability for initially randomly distributed particles is given by[7,40]

$$\mathcal{S}(t|eq) = \exp[-cP(*;t|eq)] \qquad (21)$$

The quantity $P(*;t|eq)$ is defined from the normalization condition

$$P(*;t|eq) \equiv \gamma_d\int_a^{x_m} [P(x;0|eq) - P(x;t|eq)]x^{d-1}\,dx \quad (22)$$

where $P(x;t|eq)$ obeys the Smoluchowski equation 5 for an initial equilibrium state (eq 6).

The main modification lies in the nonlinear boundary condition

$$\gamma_d D a^{d-1} e^{-V(a)} \frac{\partial}{\partial x} e^{V(x)} P(x;t)|_{x=a} =$$

$$\kappa_a P(a;t) - \kappa_d [\exp(cP(*;t)) - 1]/c \quad (23)$$

It reduces to the back-reaction boundary condition (eq 10) in the infinite dilution limit, $c \rightarrow 0$. In this limit, eq 21 gives $cP(*;t) \rightarrow 1 - S(t|eq)$. Indeed, for a single pair, $c = 1/v$, v being the system's volume; hence $cP(*;t) = p(*;t)$ is the single-pair binding probability. When $\kappa_d = 0$, the definition of $k(t)$ (eq 7) implies that

$$P_{irr}(*;t|eq) = \int_0^t k(t') \, dt' \quad (24)$$

and therefore eq 21 reduces to the Smoluchowski result for irreversible recombination (eq 1). In the limit of an infinite system ($x_m \rightarrow \infty$) one can show[40] that the SA tends to the correct equilibrium limit (eq 12a). In the limit of small cK_{eq} it approaches equilibrium as[7]

$$S_{eq} - S(t|*) \sim [K_{eq}/(1 + cK_{eq})](4\pi Dt)^{-d/2} \quad (25)$$

For one-dimensional binding on half the line, where the trap is approached only from one side, the above result should be multiplied by 2. To obtain SA results for the initially bound state we have applied the GMA law to the initially unbound state. It is not possible to calculate this case directly, since the SA cannot be written for the bound initial state.

IV. Simulation

A. Technical Detail. We have simulated up to $N = 1000$ randomly-moving particles on the half-line with a static trap at the origin. An example of such a simulation is shown in Figure 3 (symbols). The trap may bind at most one particle. The particles are initially randomly distributed on the interval $[0,L]$. Its length, L, is sufficiently large to ensure achievement of the thermodynamic limit, as previously demonstrated.[38] The particle concentration is thus $c \equiv N/L$. The diffusion coefficient, D, and the recombination parameter, κ_r, are arbitrarily set to unity. This is equivalent to choosing time and distance scales. The dissociation parameter, κ_d, was varied. Results were converted to the initial condition of an occupied trap using the (exact) GMA relation (eq 15).

The data in Figure 3 show the approach to equilibrium, $S_{eq} - S(*|t)$, for over 6 orders of magnitude in time. The short-time behavior was also calculated from lattice random walks (RWs), using the algorithm of ref 9. Obtaining the behavior at long times required the development of a many-body Brownian dynamics algorithm.[38] This is an off-grid (continuous space) method that utilizes the exact one-particle solution (which for $d = 1$ is known analytically) in propagating a many-particle trajectory. The underlying assumption is that a chosen particle may be moved for a finite time interval, Δt, while keeping the other particles immobile. The figure shows data for eight different values of Δt. The simulation is inaccurate for times on the order of Δt, but convergence to the correct result is so rapid that for $t > 5\Delta t$ the data agree with that obtained using a smaller time step. Therefore, the short-time tails are spliced off and the data for different Δt values are connected to produce the behavior over the entire time regime (thin line).

As expected, the closer the survival probability to its equilibrium limit, the larger the statistical noise, so that more stochastic trajectories are required to collect reasonable statistics. For example, the longest time segment shown in Figure 3, $\Delta t = 500$, involves averaging over about 4 million trajectories. One thousand trajectories of length 50 Δt take $10-15$ min on a 2.5 MFLOPS 486 PC. In the other limit, of short times,

relatively few trajectories need be averaged but Δt has to be extremely small. We verify the short-time data by comparison with conventional RW results.[9]

B. Concentration Series. We have performed a series of simulations to demonstrate the effect of varying the concentration for a fixed dissociation parameter, $\kappa_d = 0.1$. In this series the interval is fixed, $L = 2500$, while the number of particles varies, $N = 5, 50, 500$, and 1000. Figure 4 shows the binding probability as a function of time on a ln−ln scale (natural logarithm). The data (bold curves) are analogous to the experimental data of Figure 1. Starting with an initially occupied trap, $1 - S(t|*)$ decreases monotonically until the equilibrium limit is approached (eq 12). The lower the concentration, c, the smaller $1 - S_{eq}$ and the equilibrium limit is approached slower. These data, previously compared only with the SA,[40] will now be confronted with all three approximations discussed in section III. The approximations are calculated using the same parameters as in the simulations, so that no adjustable parameters are involved.

The calculation verifies the convergence properties deduced theoretically. The MRE, which does not tend to the correct solution in the infinite dilution limit, indeed performs very poorly at low concentrations, except when $t \rightarrow 0$ or $t \rightarrow \infty$. In contrast, both CA and SA reduce to the correct infinite dilution behavior, as expected theoretically. However, the SA converges better near $c = 0$, e.g., for $c = 0.02$ it is essentially exact. At high concentrations all three approximations seem to agree with the simulation. However, a closer look at the way they approach equilibrium reveals differences.

Figures 5 and 6 show the deviation from equilibrium obtained by subtracting the exact equilibrium limit (eq 12a) from both simulation and approximations. The short-time behavior is shown on a semi-ln scale in Figure 5 and the complete time behavior on a ln−ln scale in Figure 6. For the given value of κ_d, the REs are inadequate even at short times. The decay to equilibrium is predominantly nonexponential. The MRE are markedly better, and the CA is better still. These approximations agree at short times, but the MRE diverges from the exact solution before the CA. While the above approximations approach equilibrium faster than the simulation, the SA becomes slower than required at long times. It follows that the two most useful approximations are the SA and CA, which bracket the simulation data from above and below, respectively.

It is also seen that both CA and SA become exact at low concentrations. For $c = 0.002$ they practically coincide with the simulated data. Figure 6 shows that the convergence properties of the SA at low c are better than those of the CA. The SA also shows the apparently correct $t^{-d/2}$ limiting behavior. Because it approaches equilibrium too slowly at intermediate times, the SA curves run parallel and above the simulation as $t \rightarrow \infty$ for high concentrations.

C. Reactivity Series. In order to bridge over the spectrum of kinetic behaviors ranging from ultrafast to ultraslow reactions, we have performed another series of simulations, where κ_d varies at a fixed value of $c = 0.4$. For large κ_d the site is mostly empty while for small κ_d the site is mostly occupied near equilibrium. Since the occupancy of the site induces correlations between bound and unbound particles, the expectation is that the large and small κ_d limits will correspond to weak and strong competition, respectively.

Figure 7 shows the time dependence of $S_{eq} - S(t|*)$ for the two largest κ_d values. The semi-ln plot in the bottom panel shows that the initial decay is approximately $\exp(-\kappa_d t)$. This is the same as the RE of eq 17, since in this limit $\kappa_d \gg c\kappa_r$ and $S_{eq} \approx 1$. For large κ_d the RE gives the correct slope at $t = 0$. Indeed, for short times and fast reactions, the density perturba-

Equilibration in Reversible Bimolecular Reactions
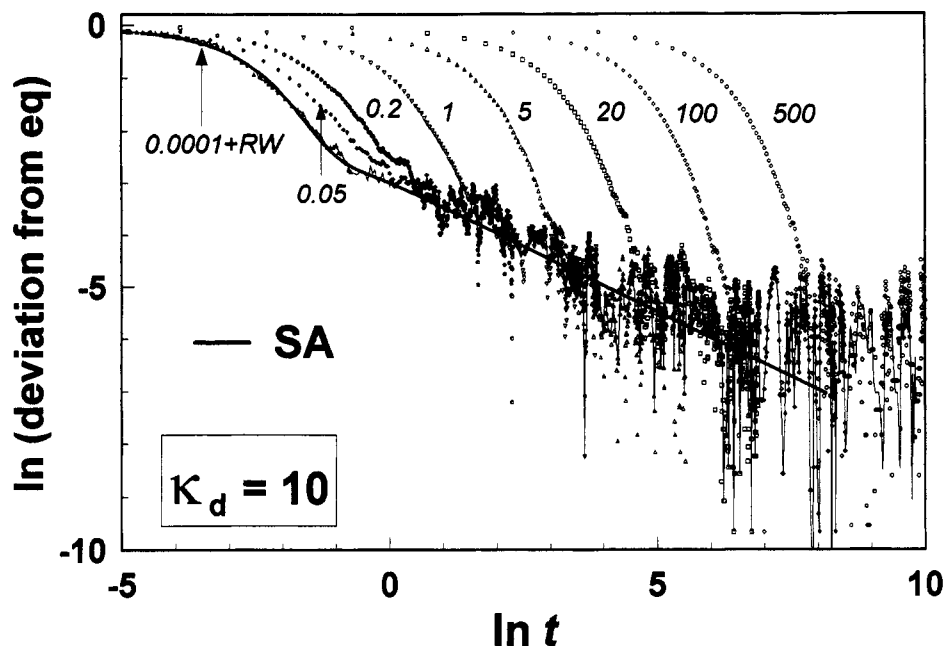
J. Phys. Chem., Vol. 99, No. 15, 1995 **5395**

Figure 3. Approach to equilibrium in one-dimensional Brownian simulations of 1000 particles on a line segment of length $L = 2500$, hence $c = 0.4$. In this and all subsequent simulations $D = 1$ and $\kappa_r = 1$. Symbols represent simulations with different time steps, Δt, as indicated. The thin line is the combined simulation result over the entire time regime. The thick curve is the superposition approximation (eq 21).
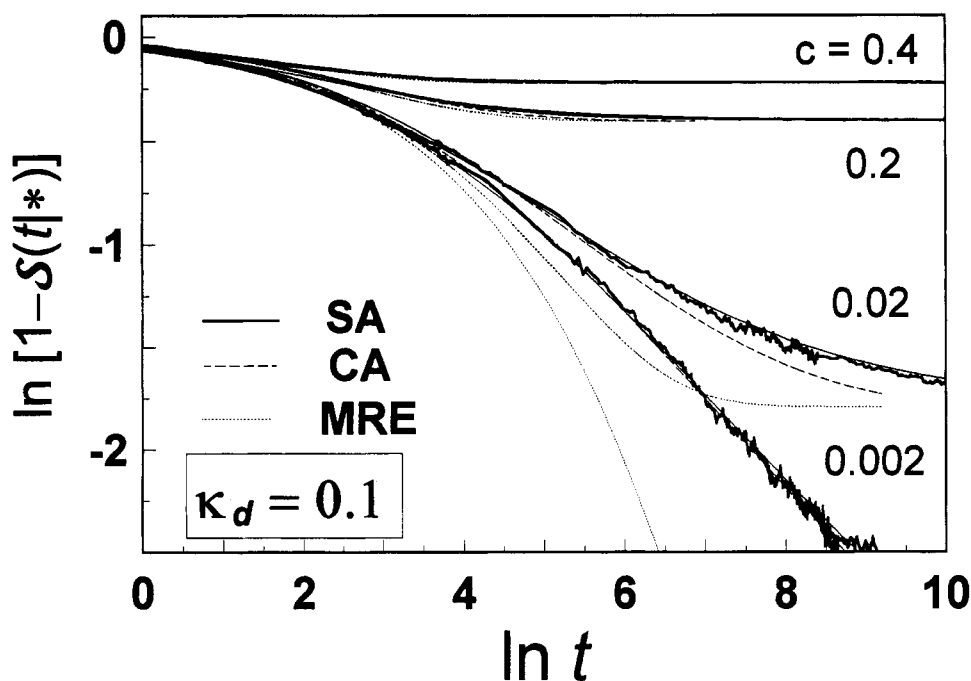
Figure 4. Concentration effects on reversible binding as revealed by 1d Brownian simulations (bold lines). The simulation is compared with three approximate theories. The parameters D, κ_r, and L are the same as in Figure 3. The number of particles, N, is varied to achieve the indicated concentration, $c \equiv N/L$.

tions near the trap are not yet propagated to large distances and competition effects had not had time to develop. In the weak competition limit much of the decay is describable in this simple way. At longer times there is a switchover to the universal power-law decay, but only a minor fraction of $\mathscr{S}_{eq} - \mathscr{S}(t|*)$ decays via this power-law mechanism. Also, the SA becomes exact in this limit, as seen in the upper panel of Figure 7.

Figures 8 and 9 show the approach to equilibrium for intermediate to small κ_d values on semi-ln and ln–ln scales, respectively. As Figure 8 demonstrates, the short-time behavior is given by the RE (eq 17) only for large κ_d. The MRE is much better and the CA better still. Again, we observe that the SA and CA bracket the exact results from above and below, respectively. It is now seen how the relative error in these two

approximations depends on the reactivity. For large κ_d the SA is the best available approximation. Indeed, it is expected to be exact when $\kappa_d \rightarrow \infty$. For small κ_d the CA (and even the MRE) are better. We suggest terming these two limiting behaviors "superposition dominated" and "convolution dominated", respectively.

As Figure 9 demonstrates, the long-time behavior is a universal $t^{-1/2}$ power law. For intermediate κ_d values (e.g., $\kappa_d = 1$) this phase seems to dominate most of the approach to equilibrium. As κ_d decreases, an intermediate-time phase emerges which is neither exponential nor power-law. It exhibits a slope which is noticeably larger than $d/2$. Consequently, the switchover to the asymptotic power-law decay becomes more conspicuous. Let us denote the switchover time by t_s. It
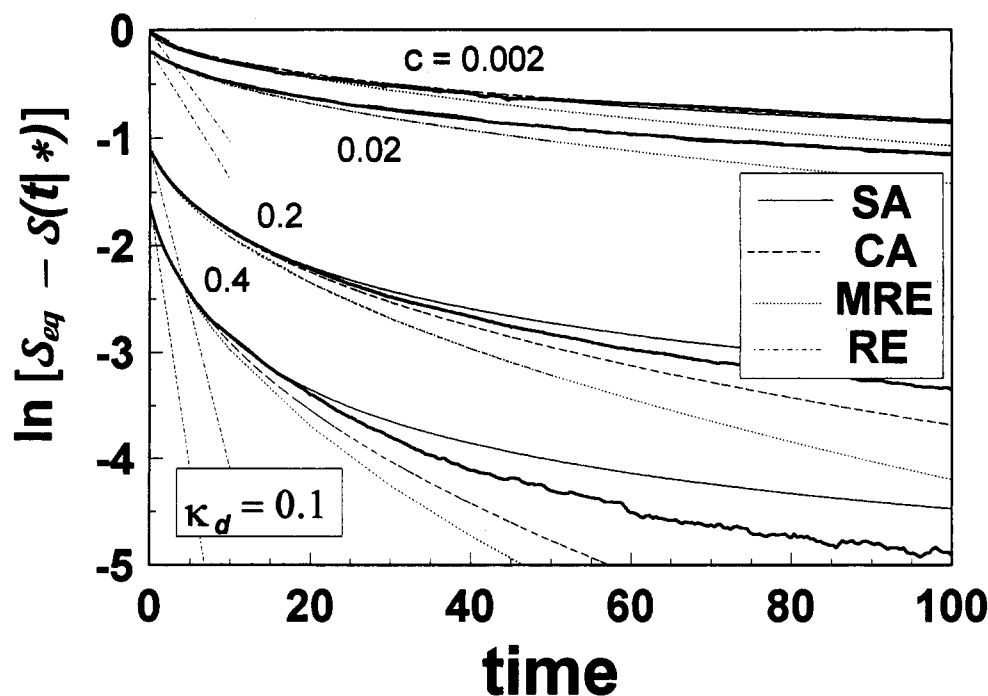
Figure 5. Approach to equilibrium in competitive reversible binding. Same data as in Figure 4, from which the exact equilibrium limit has been subtracted (thick lines).
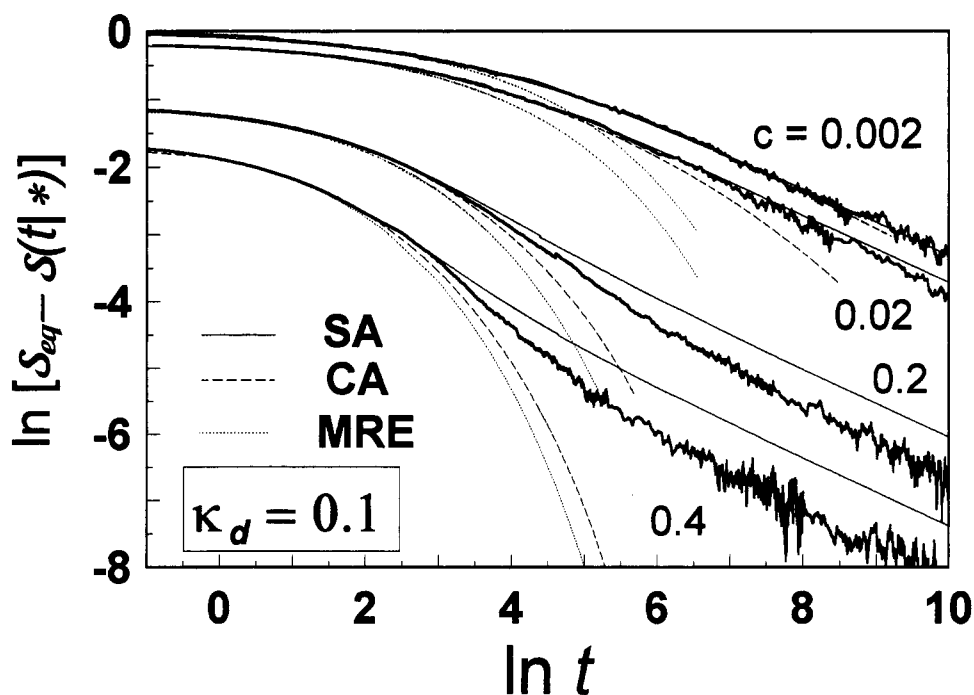

Figure 6. Same as Figure 5 on a (natural) double logarithmic scale.

increases monotonically with κ_d. Interestingly, for slow dissociation, $t_s \approx 1/\kappa_d$.

V. Experiment

A. Excited-State Proton Transfer to Solvent. The experiment[3] monitors the transient time-correlated single-photon counting (TCSPC) fluorescence signal from excited HPTS molecules as they transfer a proton reversibly to water

$$R^*OH \rightleftharpoons R^*O^- + H^+ \qquad (26)$$
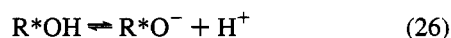
Here R*OH symbolizes the acidic form of excited HPTS, R*O⁻ is its basic form, and H⁺ is the solvated proton. A picosecond laser pulse produces vibrationally hot R*OH in S_1. It cools

very fast and begins to dissociate within about 100 ps. Its fluorescence signal is multiplied by $\exp(t/\tau_f)$, to correct for the finite radiative lifetime, τ_f. The resulting signal, shown in Figure 1, is thus the probability of the bound state, $1 - \mathcal{S}(t|*)$.

The parameters previously used in fitting the geminate pair data[3] are collected in Table 1. This limit of zero homogeneous particles, $c \rightarrow 0$, prevails at pH > 3.5, where homogeneous protons are on the average too far to interact with the anion, R*O⁻, on the experimental time scale. Of these parameters, only κ_d and κ_r were adjusted to fit the geminate-pair data. The radiative lifetime, τ_f, is obtained from the anion fluorescence signal, D and R_D are known from conductivity and dielectric measurements, and a is a customary value in the literature.
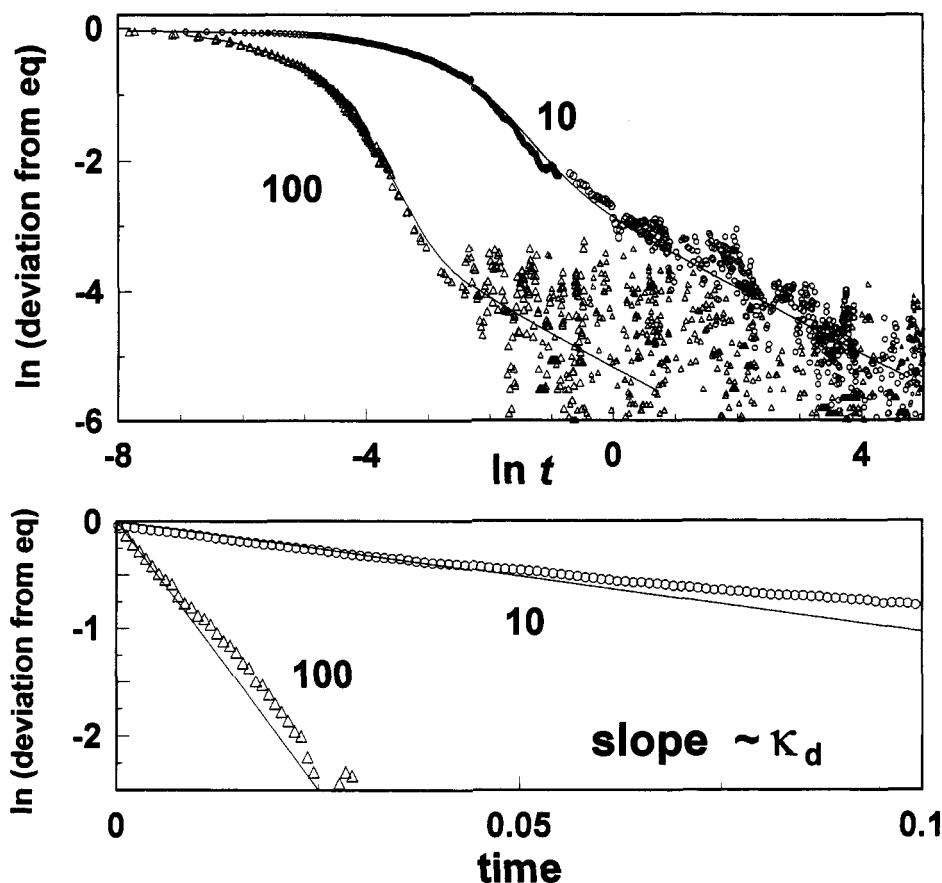
Figure 7. Reactivity effects in 1d Brownian simulations of reversible binding (symbols). Parameters are identical to those of Figure 3, except that κ_d is varied as indicated. The deviation from equilibrium, $S_{eq} - S(t|*)$, is compared in the upper panel with the SA and in the lower panel with the RE. See text for detail.

TABLE 1: Parameters Used in Comparing with the Experimental Data[3] Are Either Known Experimental Quantities or Obtained by Fitting the $c = 0$ Limit

parameter	value	units
κ_d	8	ns^{-1}
κ_r	7.4	Å/ns
τ_f	5.3	ns
D	930	Å²/ns
R_D	28.3	Å
B	2.0	$M^{-1/2}$
a	7.0	Å

As the pH is lowered below 3, homogeneous protons start competing with the geminate dissociated proton for rebinding. Unfortunately, we do not have three-dimensional simulations but may compare the experimental data to the mean-field approximations. These approximations require the solution of an effective single-particle Smoluchowski equation. Assuming that adding protons does not affect the intrinsic rate parameters, we use the *same* parameters as obtained in the high-pH limit (Table 1). Proton self-screening is described by the Debye–Hückel screening function, see the Appendix. This potential of mean force is accurate at low concentrations. Fortunately, the concentrations required for observing the many-body effects (<10 mM) are within its applicability range.

The theoretical curves *have not* been convoluted with the "instrument response function" (IRF). Its width, 50–60 ps, has a negligible effect on the data for $t > 100$ ps. Unfortunately, the IRF has a small satellite peak around $t = 0.3$ ns (log $t = -0.5$). Its amplitude is a few percent of the main peak (see Figure 1 in ref 45), leading to the small hump in the experimental data around 300 ps. Since this produces deviations which are small in comparison with differences between the

various approximations, we felt it was not justified to distort the theoretical curves by convolution.

B. Comparison with Approximations. Figure 1 has compared HPTS data with the RE and MRE approximations, showing unsatisfactory agreement. The RE constitutes the most drastic approximation considered here. It is expected to hold only in the limit that both κ_d and κ_a are small as compared with D. The MRE, which involves time-dependent rate coefficients (eq 18), is a noticeable improvement at high concentrations but still rather poor for small c. It always approaches equilibrium *faster* than experiment. The same behavior was observed in comparing the MRE with the 1d simulations (Figure 6).

Figure 10 shows that the CA and SA perform considerably better than the various rate equations. These mean-field approximations are calculated for a three-dimensional system and a Debye–Hückel potential of mean force without adjusting any parameter. They are a realistic description of the reaction, except that the many-body effect is treated only approximately. In evaluating the CA, we use $k(t)$ from eq 8b, which is inaccurate for small t when $V(x) \neq 0$. At short times, the experiment is not a faithful delta-function response due to the secondary peak in the IRF (see above), so that its agreement with the CA is coincidental. Thus the SA depicts the correct short-time behavior in this case. At long times the SA and CA slightly underestimate the ultimate equilibrium limit (e.g., for $c = 4$ mM). This could be due to inaccuracies in the DH potential. At the highest concentrations both CA and SA seem to perform equally well.

The two approximations differ, however, in their approach to equilibrium shown in Figure 11. For $c > 0$, the SA is always above the experimental data. This resembles the 1d simulations in Figure 6. In contrast, the CA is quite close to the
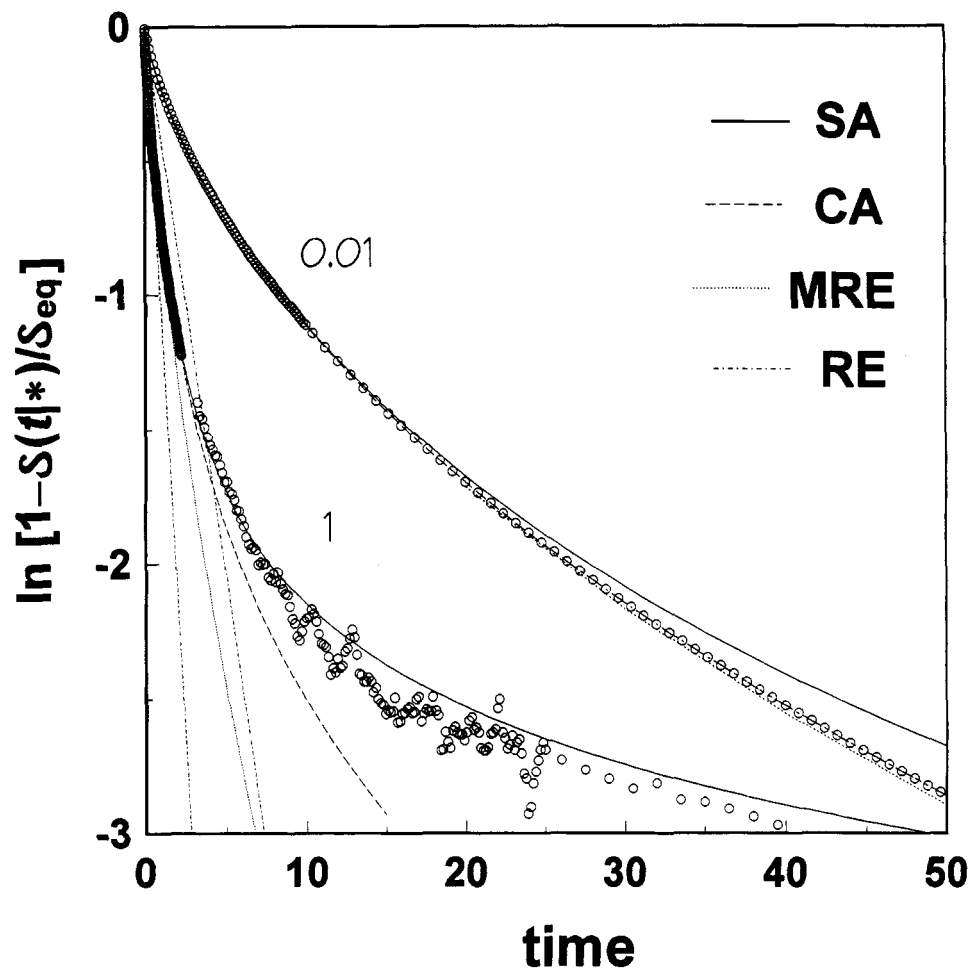
Figure 8. Same as Figure 7 (lower panel) for smaller κ_d values (indicated). The simulation data (symbols) are compared with four approximations.

experimental data. This might indicate that for large c the CA becomes more accurate with increasing dimensionality.

The HPTS data apparently correspond to the intermediate rather than the asymptotic time regime. The slopes of the measured curves for large concentrations are larger than $^3/_2$. If these measurements could be extended to longer times with good signal/noise ratios, we expect to see a crossover to the asymptotic power-law behavior resembling that of Figure 9.

VI. Conclusion

More than a century after Arrhenius, it is surprising to discover how little of chemical kinetics we really understand.

A widespread misconception is that the time course of a reaction essentially obeys an appropriate form of a rate equation, so that the main problem is to determine, from first principles if possible, the magnitude of the reaction rate coefficients. Much of current day study of chemical kinetics, from gas-phase dynamics to surface reactions, centers on understanding the factors governing rate coefficients. While such studies are of fundamental interest and importance, the concomitant neglect of a more rigorous and comprehensive study of the time course of chemical reactions is unjustified.

Bimolecular chemical kinetics is complicated because it represents a many-body problem. Nonequilibrium distributions of reacting particles and their competition over binding sites may have marked effects on the reaction course, particularly in fast reactions in which reversibility cannot be neglected. One might expect that, in a system containing many particles, mean-field theories should be adequate. This depends on the level of the mean-field approximation. The traditional rate equations completely neglect the microscopic individuality of the reacting

particles and their spatial distribution. They are incapable of explaining the simulation or experimental data. More refined mean-field theories with microscopic origin, like the CA and SA, are quite successful in reproducing correctly various limiting behaviors, such as at long times, low concentrations, and slow and fast dissociations. However, even these theories are incapable of reproducing all the details revealed by the Brownian simulations.

Until recently it was not possible to explore the full spectrum of feasible behaviors. The many-particle Brownian simulation technique has allowed us to perform a systematic search of parameter space, albeit only in one dimension (1d). It is nevertheless often the case that 1d systems provide the most stringent test for approximate kinetic theories. Simulations in 1d are easier to perform and, in addition, the number of independent physical parameters is smaller. Because the contact distance between two points is zero, there is no natural distance scale, so that an arbitrary determination of D and κ_r is equivalent to setting the time and distance scales. The transient behavior is then determined by κ_d and c. We have therefore performed two series of simulations, a concentration and reactivity series, which together paint a rather complete picture of the situation in 1d.

Our simulations demonstrate that pseudo-unimolecular reactions may show up to three phases in their transient behavior. The short-time behavior resembles the exponential decay predicted by chemical rate equations when κ_d is large. The long-time behavior seems always to be a universal power law, indicative of diffusional motion. Under strong competition conditions, an intermediate phase emerges, with faster than
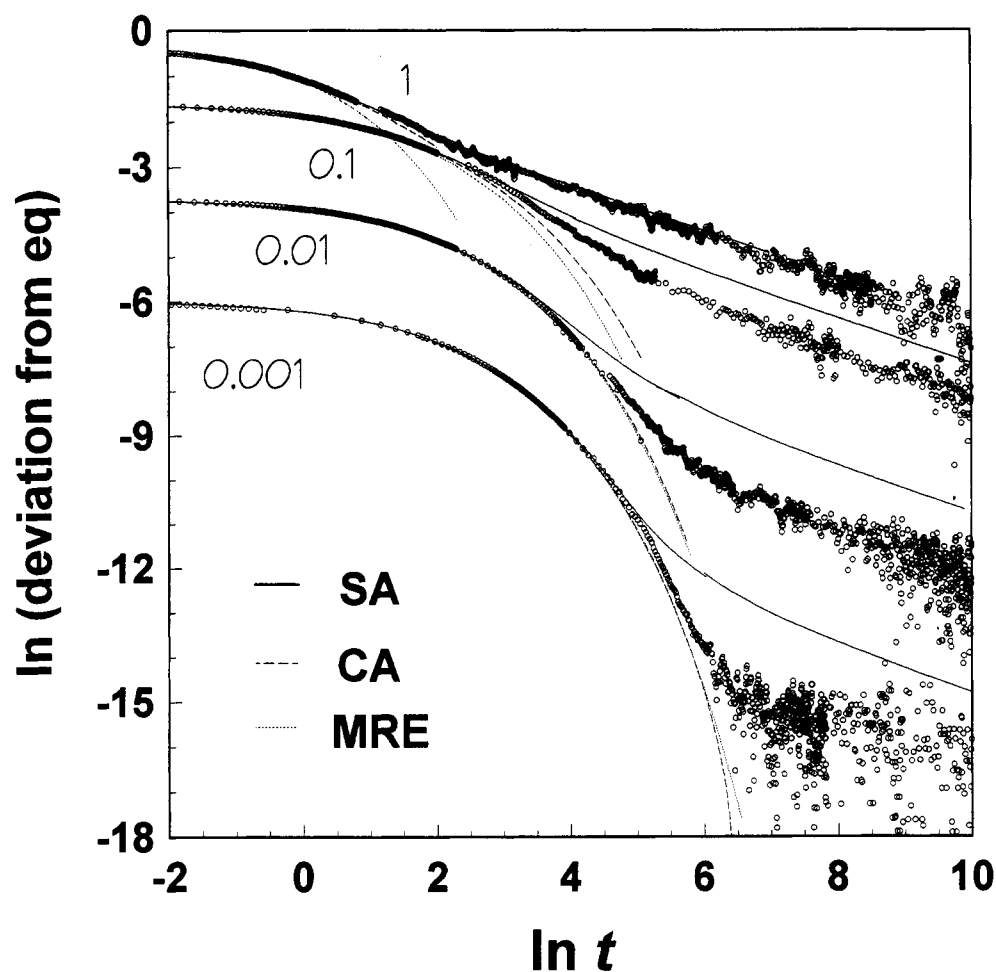
Equilibration in Reversible Bimolecular Reactions

J. Phys. Chem., Vol. 99, No. 15, 1995 **5399**

Figure 9. Same as Figure 8 for four κ_d values and a ln—ln scale.
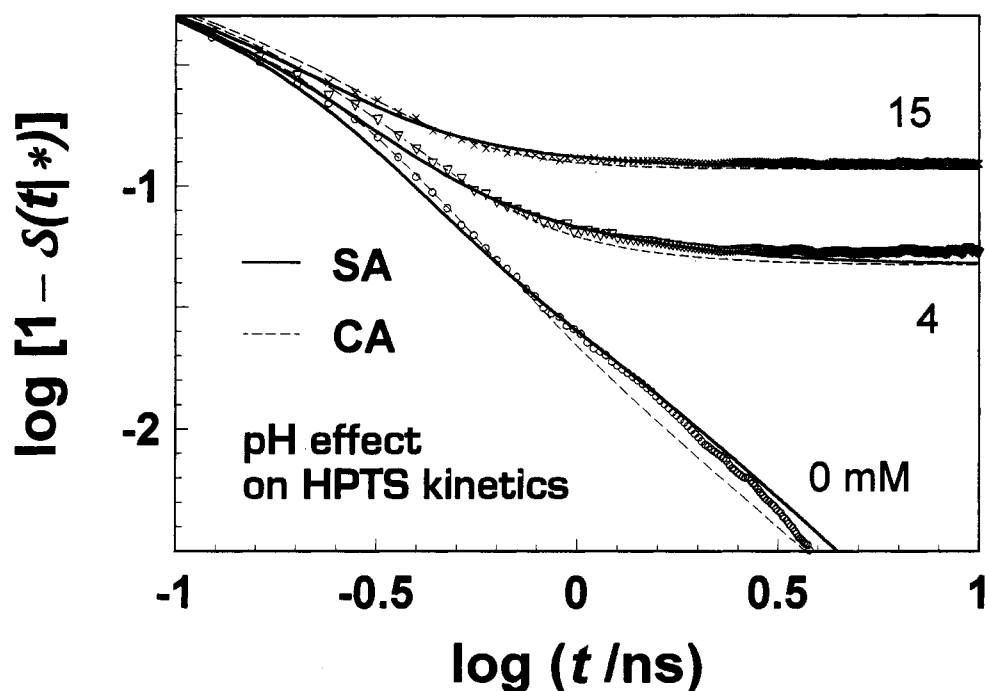

Figure 10. Experimental data of Figure 1 as compared with the two more sophisticated approximations. Parameters are listed in Table 1.

power law approach to equilibrium. Subsequently, we assign this phase to the competition effect.

In 3d, the contact distance $a > 0$, already sets the distance scale so that both κ_r and κ_d may be independently varied. One may envision a situation where both are small with respect to D. This is the "reaction control" limit in which rate equations

are expected to dominate. The opposite case where both rate parameters are large as compared with D is expected to be "superposition dominated". Additionally, one may consider the cases when one rate coefficient is large and the other small. If κ_d is the small rate parameter the problem reduces (save at very long times) to irreversible recombination. Little is known about
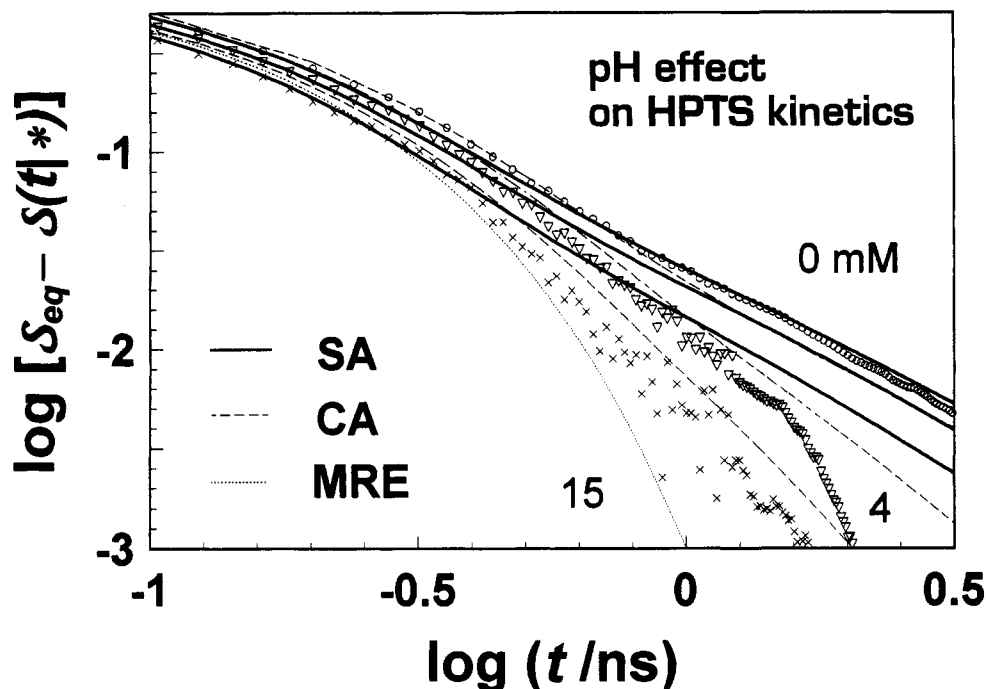
Figure 11. Approach to equilibrium of the experimental data (symbols), obtained by subtracting the asymptotic limit from the data of Figure 10 and applying some numerical smoothing, as described in ref 3. The MRE is shown only for $c = 15$ mM.

the opposite limit of small κ_r and large κ_d. In addition, the behavior in each of these limits varies with c. To fully explore this richness of possible behaviors, a three-dimensional simulation project is required.

Rather than waiting until 3d simulations become available, we have proceeded to apply the lessons learned from 1d simulations to experiment. An interesting unexplained observation in the HPTS data[3] was the increase of the long-time slope with increasing concentration. From the Brownian simulations it seems that these data may indeed reflect many-body effects in fast, reversible chemical reactions. This follows because the relation between various approximations, MRE, CA, and SA, and the experimental data closely resembles the behavior observed in the 1d simulation. The simulations indeed exhibit faster approach to equilibrium at intermediate times and high concentrations, which correlates with increasing deviations from the above approximations. The large sensitivity and dynamic range of the TCSPC system are insufficient to cover all three transient phases revealed by the simulations because at longer times there should be a crossover into the asymptotic $t^{-3/2}$ behavior. It would be interesting if the experimental technique could be further perfected to detect this switchover.

While pH variations yield a "concentration series", it may also be possible to obtain a "reactivity series" involving a variation of κ_d. For example, changing the solvent from water to a 50/50 mixture of methanol—water is known[45] to diminish κ_d by an order of magnitude, while reducing κ_r and D by only a factor of 2. Monitoring the pH effect on this reversible reaction in water—alcohol mixtures may thus allow one to span a much larger reactivity range than in pure water. We expect to observe a more drastic switchover into the universal power-law behavior in these solvents, see Figure 9.

Finally, proton transfer across and between membranes is an essential step in oxidative phosphorylation, leading to the synthesis of ATP from ADP. In this process, a transmembranal proton gradient is utilized for energy storage. While little is known about the elementary microscopic steps, they undoubtedly include proton diffusion and binding to membrane proteins. The HPTS system has been applied successfully in the study of reversible geminate recombination between membranes and

within biological cavities.[46,47] It would be interesting to extend such studies to low pH values in order to monitor many-body effects within spatially restricted cavities.

Appendix: The DH Potential

Since the experiment involves ions, the potential applied is the screened Coulomb potential of Debye and Hückel[48]

$$V(r) = - \frac{R_D}{r} \frac{\exp[-\kappa_{DH}(r - a)]}{1 + \kappa_{DH}a} \qquad (27)$$

Here R_D is the Debye (sometimes, Onsager) radius

$$R_D \equiv |z_1 z_2| e^2/(\epsilon k_B T) \qquad (28a)$$

where z_i are the ionic charge numbers (-4 and $+1$ for the HPTS proton pair, since the HPTS anion has three charged sulfonate groups), e is the electronic charge, and ϵ is the static dielectric constant. Taking $\epsilon \approx 80$ for water one obtains for the HPTS proton pair at room temperature $R_D = 28.3$ Å. κ_{DH}^{-1} is the radius of the "ionic atmosphere". For a $1-1$ electrolyte (the added acid) of concentration c it is given by

$$\kappa_{DH}^2 \equiv (8\pi e^2 c)/(\epsilon k_B T) \qquad (28b)$$

For room temperature water $\kappa_{DH} = 0.328 c^{1/2}$ Å, when c is in molar. Taking for the contact radius, as customary[49] $a = 7$ Å, we get

$$\kappa_{DH} a = B c^{1/2} \qquad (28c)$$

with $B = 2.3$ M$^{-1/2}$. Unfortunately, the DH potential is only a mean-field approximation for the many-particle interaction potential, which breaks down at ionic concentrations above a

Equilibration in Reversible Bimolecular Reactions

J. Phys. Chem., Vol. 99, No. 15, 1995 **5401**

few millimolar. To compensate for this, we modify B to a value suggested by Weller,[49] $B = 2.0$ M$^{-1/2}$. Up to $c = 15$ mM (the largest concentration in Figure 1) this correction produces reasonable values of $\mathcal{J}(\infty)$, namely, a correct "equilibrium salt effect".

References and Notes

(1) Rice, S. A. *Diffusion-Limited Reactions*; Comprehensive Chemical Kinetics; Elsevier: Amsterdam, 1985; Vol. 25.

(2) Laidler, K. J. *Chemical Kinetics*, 3rd ed.; Harper and Row: New York, 1987.

(3) Huppert, D.; Goldberg, S. Y.; Masad, A.; Agmon, N. *Phys. Rev. Lett.* **1992**, *68*, 3932.

(4) Pines, E.; Huppert, D.; Agmon, N. *J. Chem. Phys.* **1988**, *88*, 5620.

(5) Agmon, N.; Pines, E.; Huppert, D. *J. Chem. Phys.* **1988**, *88*, 5631.

(6) Huppert, D.; Pines, E.; Agmon, N. *J. Opt. Soc. Am. B* **1990**, *7*, 1545.

(7) Szabo, A. *J. Chem. Phys.* **1991**, *95*, 2481.

(8) Keizer, J. *Chem. Rev.* **1987**, *87*, 167.

(9) Agmon, N.; Schnörer, H.; Blumen, A. *J. Phys. Chem.* **1991**, *95*, 7326.

(10) Blumen, A.; Zumofen, G.; Klafter, J. *J. Phys.* **1985**, *46*, C7.

(11) Szabo, A.; Zwanzig, R.; Agmon, N. *Phys. Rev. Lett.* **1988**, *61*, 2496.

(12) Tachiya, M. *Radiat. Phys. Chem.* **1983**, *21*, 167.

(13) Szabo, A. *J. Phys. Chem.* **1989**, *93*, 6929.

(14) Gösele, U. M. *Prog. React. Kinet.* **1984**, *13*, 63.

(15) Kuzovkov, V.; Kotomin, E. *Rep. Prog. Phys.* **1988**, *51*, 1479.

(16) Argyrakis, P.; Kopelman, R.; Lindenberg, K. *Chem. Phys.* **1993**, *177*, 693.

(17) Agmon, N. *Phys. Rev. E* **1993**, *47*, 2415.

(18) Lee, S.; Karplus, M. *J. Chem. Phys.* **1987**, *86*, 1883.

(19) Sienicki, K.; Winnik, M. A. *J. Chem. Phys.* **1987**, *87*, 2766.

(20) Martinho, J. M. G.; Winnik, M. A. *J. Phys. Chem.* **1987**, *91*, 3640.

(21) Vogelsang, J.; Hauser, M. *J. Phys. Chem.* **1990**, *94*, 7488.

(22) Vogelsang, J.; Hauser, M. *Ber. Bunsen-Ges. Phys. Chem.* **1990**, *94*, 1326.

(23) Xu, R.; Winnik, M. A. *J. Photochem. Photobiol. A* **1991**, *57*, 351.

(24) Berberan-Santos, M. N.; Martinho, J. M. G. *J. Chem. Phys.* **1991**, *95*, 1817.

(25) Berberan-Santos, M. N.; Martinho, J. M. G. *Chem. Phys. Lett.* **1991**, *178*, 1.

(26) Burlatsky, S. F.; Oshanin, G. S.; Ovchinnikov, A. A. *Chem. Phys.* **1991**, *152*, 13.

(27) Keizer, J. *J. Am. Chem. Soc.* **1990**, *112*, 7952.

(28) Molski, A.; Keizer, J. *J. Chem. Phys.* **1992**, *96*, 1391.

(29) Molski, A. *Chem. Phys. Lett.* **1992**, *191*, 59.

(30) Naumann, W. *Chem. Phys.* **1991**, *150*, 187.

(31) Naumann, W. *J. Chem. Phys.* **1993**, *98*, 2353.

(32) Naumann, W.; Molski, A. *J. Chem. Phys.* **1994**, *100*, 1511.

(33) Molski, A.; Naumann, W. *J. Chem. Phys.* **1994**, *100*, 1520.

(34) Richards, P. M. *J. Chem. Phys.* **1990**, *92*, 1963.

(35) Agmon, N.; Szabo, A. *J. Chem. Phys.* **1990**, *92*, 5270.

(36) Szabo, A.; Zwanzig, R. *J. Stat. Phys.* **1991**, *65*, 1057.

(37) Richards, P. M.; Szabo, A. *J. Stat. Phys.* **1991**, *65*, 1085.

(38) Edelstein, A. L.; Agmon, N. *J. Chem. Phys.* **1993**, *99*, 5396.

(39) Edelstein, A. L.; Agmon, N. In *Ultrafast Reaction Dynamics and Solvent Effects*; Gauduel, Y., Rossky, P. J., Eds.; AIP Conference Proceedings 298; New York, 1994; pp 473−484.

(40) Agmon, N.; Edelstein, A. L. *J. Chem. Phys.* **1994**, *100*, 4181.

(41) Lamm, G.; Schulten, K. *J. Chem. Phys.* **1981**, *75*, 365.

(42) Lamm, G.; Schulten, K. *J. Chem. Phys.* **1983**, *78*, 2713.

(43) Davis, M. E.; Madura, J. D.; Sines, J.; Luty, B. A.; Allison, S. A.; McCammon, J. A. *Methods Enzymol.* **1991**, *202*, 473.

(44) Miers, J. B.; Postlewaite, J. C.; Zyung, T.; Chen, S.; Roemig, G. R.; Wen, X.; Dlott, D. D.; Szabo, A. *J. Chem. Phys.* **1990**, *93*, 8771.

(45) Agmon, N.; Huppert, D.; Masad, A.; Pines, E. *J. Phys. Chem.* **1991**, *95*, 10407. Erratum. *Ibid.* **1992**, *96*, 2020.

(46) Gutman, M.; Nachliel, E.; Kiryati, S. *Biophys. J.* **1992**, *63*, 281.

(47) Shimoni, E.; Tsfadia, Y.; Nachliel, E.; Gutman, M. *Biophys. J.* **1993**, *64*, 472.

(48) Robinson, R. A.; Stokes, R. H. *Electrolyte Solutions*, 2nd ed.; Butterworth: London, 1959.

(49) Weller, A. *Prog. React. Kinet.* **1961**, *1*, 189.